Metabolomics (2014) 10:975–985
DOI 10.1007/s11306-014-0626-1

ORIGINAL ARTICLE

Metabolic profiling of cervical tubercular lymphadenitis tissues by proton HR-MAS NMR spectroscopy

Suruchi Singh · Shatakshi Srivastava · Raja Roy · Kushagra Gaurav · Surender Kumar · Abhinav A. Sonkar · Madhu M. Goel · Rajiv Garg

Received: 8 November 2013 / Accepted: 25 January 2014 / Published online: 9 February 2014

Abstract Proton metabolic profiling of incisional biopsied cervical lymph node tissue specimens of 109 patients suffering from tubercular (CTBL) and non-specific (NSCLA) lymphadenitis were analyzed by high resolution magic angle spinning (HR-MAS) NMR spectroscopy. In the present study, 40 endogenous metabolites namely, myo-inositol (m-Ins), branched chain amino acids (BCAA), glutamate, serine, taurine (Tau) aromatic amino acids, choline (Cho) containing compounds and glucose were characterized. To the best of our knowledge, this is the first report on metabolic profiling of cervical tubercular lymph node tissues using HR-MAS NMR spectroscopy. The principal component analysis revealed a clear discrimination between CTBL and NSCLA tissues. Increase in the concentration of mobile poly unsaturated fatty acids, BCAA, Cho, Tau, glycine and a decrease in the concentration of lactate, phosphocholine and m-Ins was observed in CTBL cases. The partial least square discriminant analysis (PLS-DA) with $R^2 = 0.95$ and $Q^2 = 0.92$ provided >98 % of correct classification between the two groups. A PLS-DA training set model of 75 % (CTBL = 54, NSCLA = 27) of the subjects when subjected for prediction of 25 % cases (CTBL = 18, NSCLA = 10) as an unknown dataset provided more than 98 % of diagnostic accuracy in their respective histological categories. The receiver operator characteristic curve was generated from PLS-DA factor-1 projected an area under the curve of 0.962. The metabolic profile obtained from HR-MAS NMR spectroscopy may be used as surrogate markers in vivo MRS for differentiating between CTBL and NSCLA cases non-invasively.

Keywords HR-MAS NMR spectroscopy · Cervical tubercular lymphadenitis · Metabolic profiling · Multivariate statistical analyses · Metabolomics

Abbreviations

CPMG	Carr–Purcell–Meiboom–Gill
CTBL	Cervical tubercular lymphadenitis
HPE	Histopathological examination
HR-MAS	High resolution-magic angle spinning
NOESY	Nuclear overhauser effect spectroscopy
NSCLA	Non-specific cervical lymphadenitis
PLS	Partial least square regression
PCA	Principal component analysis
ROC	Receiver operator characteristic
TB	Tuberculosis
TNF-α	Tumor necrosis factor-α

Electronic supplementary material The online version of this article (doi:10.1007/s11306-014-0626-1) contains supplementary material, which is available to authorized users.

S. Singh · S. Srivastava · R. Roy (✉)
Centre of Biomedical Research formerly known as Centre of Biomedical Magnetic Resonance, SGPGIMS Campus, Raibarely Road, Lucknow 226014, Uttar Pradesh, India
e-mail: roy@cbmr.res.in

K. Gaurav · S. Kumar · A. A. Sonkar (✉)
Department of General Surgery, King George's Medical University, Lucknow 226003, Uttar Pradesh, India
e-mail: abhinavarunsonkar@gmail.com

M. M. Goel
Department of Pathology, King George's Medical University, Lucknow 226003, Uttar Pradesh, India

R. Garg
Department of Pulmonary Medicine, King George's Medical University, Lucknow 226003, Uttar Pradesh, India

1 Introduction

Tuberculosis (TB) is one of the most widespread infectious diseases and a leading cause of death from a single infectious agent among adults globally (De Cock 2006). It remains a major global public health problem. While the developing countries are still striving to conquer the disease, it has staged its resurgence in the developed world due to HIV infection and multidrug resistance acquired by the infectious agent (Jain 2011). The World Health Organization (WHO) estimated, 9.4 million incidences and 1.7 million deaths worldwide in 2009 which makes TB a global threat (World Health Organization. Global tuberculosis control 2010). The organization has declared TB as a global emergency. The number of global cases is still increasing in absolute terms, in developing countries (Shahzad and Kohler 2009). This may be due to population growth and high prevalence of the pandemic human immunodeficiency virus (HIV) in these regions (Corbett et al. 2003). India has the highest number of TB cases in the world (Global Tuberculosis control, WHO Report 2009).

Tuberculosis in the human population is mainly caused by *Mycobacterium tuberculosis* (Mtb). TB infection can be of pulmonary or extra pulmonary type. Extra pulmonary tuberculosis (EPTB) accounts for approximately 15 % of all TB infections and occurs in up to 50 % of patients with HIV-TB-co-infection. The annual incidence rate of EPTB has increased all over the world in the last few years (Purohit et al. 2007). In India, EPTB comprises 20 % of all TB cases, with the mortality rate more than 4,000 in both pulmonary and extra pulmonary TB-related illnesses (Wright et al. 2008; Eshete et al. 2011). Although, the respiratory system remains the primary disease site, TB also increasingly affects other parts of the body, such as the central nervous system (CNS) (Gupta and Roy 1999; Gupta et al. 2001), gastrointestinal tract, peritoneum, lymph nodes, kidneys, and other solid viscera (Zhang et al. 2011). Clinically, the disease presents itself in protean ways and is usually diagnosed via histological examination (Purohit et al. 2007).

CTBL is the most common cause of extra-pulmonary manifestation of TB among all ethnic groups (Geldmacher et al. 2002). The disease involves the cervical lymph nodes followed by mediastinal axillary, mesenteric, hepatic portal, perihepatic and inguinal lymph nodes. If CTBL remains untreated, it may further lead to morbidity and mortality. It remains a diagnostic as well as a therapeutic challenge as it mimics pathological processes such as non-infective hyperplasia and other viral, bacterial and fungal infections. In most of these instances, the histological appearance of the nodes is entirely non-specific i.e. different etiologies are associated with similar microscopic appearance. These nodes are defined as NSCLA on histopathological examination (HPE) of incisional biopsied tissue specimens. The patients are usually being treated using a combination of anti-inflammatory and antibiotics/antifungal drugs. Cervical lymphadenitis is also less frequently observed in auto-immune reaction; sarcodiosis and parasitic infection; toxoplasmosis and HIV infection. Therefore, diagnosis of cervical lymphadenitis yields little in the form of physical and laboratory findings (Wong et al. 2013). Cervical lymphadenitis due to neoplasm's (lymphoma, sarcoma or metastatic carcinoma) is associated with a different pathology, where different organs are involved along with lymph nodes inflammation (Attie et al. 1993; Davies et al. 2008; Ahuja et al. 2008; Lindberg 1972). The diagnosis of CTBL still remains a challenge because of its diverse display and insidious onset which does not bring the patient to the physician at an early stage of the disease (Jain 2011). It often requires a combination of fine needle aspiration cytology (FNAC) or polymerase chain reaction (PCR), along with HPE. Among these, HPE is considered as a gold standard technique (Thangappah et al. 2011), as both FNAC and PCR have certain shortcomings. The FNAC has a high rate of non-diagnostic sampling with negative diagnoses and incomplete classification of various diseases although PCR is a very sensitive, but it always has a risk of contamination of the culture (Uphoff and Drexler 2011).Thus, the delay in the diagnosis of CTBL is due to the absence of typical clinical features and often negative conventional diagnostic tests due to paucibacillary nature of the samples (Jain 2011). Therefore, rapid molecular diagnostic methods are needed for differentiating between CTBL and NSCLA for proper treatment.

High resolution NMR spectroscopy is now a well-established analytical technique for obtaining information regarding the metabolic profile of body fluids and tissue extracts (Giskeødegard et al. 2010; Choi et al. 2012). Our earlier NMR spectroscopic studies for differential diagnosis of tuberculomas in adults and meningitis in children (Subramanian et al. 2005, 2008) revealed the presence of cell wall components of Mtb in cerebrospinal fluid and lipid extracts of the tissue specimens. Recently, HR-MAS NMR spectroscopy has been successfully applied to lung tissues in an experimental pulmonary TB infected animal model (Somashekar et al. 2011) for metabolic profiling followed by pattern recognition statistical techniques. They demonstrated a comprehensive metabolic profiling of various components in tissue specimens, reflecting levels of endogenous metabolites/biomarkers involved in key cellular pathways, which indicate physiological status during the progression of the disease and further it can be used in

differential diagnosis. HR-MAS NMR spectroscopy has several advantages over NMR analysis of soluble tissue extracts. The HR-MAS NMR analysis of the tissue extracts maintains the integrity of the tissue specimens and allows simultaneous detection of both lipids and small metabolites with a resolution comparable to that of solution state NMR. On the other hand, the extraction procedure requires large quantity of samples and increases the chance of loss of some low concentrated metabolites or reduction in their intensity which leads to the misinterpretation of the data (Cheng et al. 1998; Duportet et al. 2011; Bharti et al. 2013). Therefore, the objective of the present study was to evaluate proton HR-MAS NMR spectroscopy as another efficient alternative diagnostic method for incisional biopsied human ($n = 109$) tissue specimens obtained from cases of non-specific and tubercular cervical lymphadenitis for understanding the metabolic derangements in these cases in conjugation with HPE, of the same tissue specimens.

2 Materials and methods

2.1 Subjects and study protocol

Lymph node specimens obtained from 109 patients (64 males and 45 females) was used for the study. It was found that the patients were suffering either from CTBL, acute non specific and chronic non tubercular granulomatous lymphadenitis during the course of collection of the samples. Incisional lymph node biopsy was done and a part of the tissue specimen was sent to the Department of Pathology for routine histopathological testing and the other part for NMR analysis. On clinical examination, it was found that none of the patients were suffering from pulmonary tuberculosis. The detailed distribution of patients in each group, mean age and gender are reported in Supplementary Table S1. All samples were flash frozen in liquid nitrogen after biopsy and stored at $-80°$ C until NMR spectra were recorded. The study had been approved by Institutional Ethics Committee, King George's Medical University Lucknow, India. The selected patients were fully informed and their consents were taken well before the investigations.

2.2 Sample preparation and acquisition

Tissue specimen stored at -80 °C were thawed at room temperature and then washed with saline deuterated water to remove blood from them. Dissected and wet weighed (32 ± 1.5 mg) tissue specimens were packed into a 4 mm ZrO_2 rotor of 50 µl capacity. 20 µl of D_2O, having 0.03 % TSP as a chemical shift reference was filled in the rotor with tissue sample for locking the spectrometer frequency. The total time for preparing the samples was around 5 min. The sample-rotor-setup was then transferred to the HR-MAS probe. After NMR analysis all the tissue specimens were fixed in formalin and later HPE was done.

2.3 NMR experimental conditions

The proton NMR spectra were recorded on Bruker Biospin Avance-III 800 MHz NMR (BrukerGmBH, Germany) spectrometer operating at a proton frequency of 800.21 using 4 mm HR-MAS $^{1}H/^{13}C/^{31}P$ triple resonance probe-head equipped with magic angle gradient accessories. The ^{1}H NMR spectra were recorded with a spinning speed of $6{,}000 \pm 2$ Hz. Sample temperature was regulated by using Bruker BCU-05 unit at 280 ± 0.5 K during the acquisition of spectra to reduce the metabolic changes (Beckonert et al. 2010). The calibration of the temperature was performed using methanol during change over to HR-MAS probe. The ^{1}H HR-MAS NMR spectra were recorded within a few days and no further temperature calibration was performed during the sample analysis.

2.3.1 One dimensional NMR analysis

The ^{1}H HR-MAS spectra with water suppression were acquired using one-dimensional single pulse and Carr–Purcell–Meiboom–Gill (CPMG) pulse sequence with the following experimental parameters: spectral width of 12,820.5 Hz, time domain data points of 64 K, effective 90° flip angle, 9.0 µs, relaxation delay 4.0 s, acquisition time of 2.55 s, 64 number of scan with 4 dummy scan, a constant receiver gain of 50.8 with a total recording time of 9 min. CPMG pulse sequence with water suppression [PRESET-90°-(δ-180°-δ)$_n$-Aq] was performed to remove short T_2 components arising due to the presence of proteins as well as to obtain a good baseline for multivariate analysis. Echo time of 40 ms ($2\delta \times n$, $n = 200$, $\delta = 100$ µs) was used in CPMG pulse sequence. All spectra were processed using line broadening for exponential window function of 0.3 Hz prior to Fourier transformation. The ^{1}H HR-MAS spectra obtained from the lymph node mass were manually phased and baseline corrected automatically using TOP-SPIN 2.1 (BrukerAnalytik, Rheinstetten, Germany). The total analysis time (including sample preparation, optimization of NMR parameters and data acquisition) of ^{1}H HR-MAS NMR spectroscopy for each sample was approximately 20 min. Usually, no significant changes in the metabolic profile are observed during this span of time. It has already been established in the earlier studies conducted by us on oral squamous cell carcinoma where no significant changes in the spectral metabolic profile was observed even after subjecting the tissue

specimens for nearly 1 h long NMR acquisitions (Srivastava et al. 2011).

2.4 Statistical analysis (data reduction and pattern recognition)

The CPMG spectra recorded were corrected for phase and baseline prior to subjecting them for multivariate analysis. The spectra were reduced to discrete chemical shift regions (between 8.8 and 0.6 ppm) with the removal of water region from 5.2 to 4.8 ppm by digitization to produce a series of sequentially integrated regions of 0.005 ppm width, using Bruker AMIX software (Version 3.8.7, Bruker Biospin, Germany). Simple rectangular binning of these regions was performed to integrate the peak area. The histograms were normalized by dividing each integral area of the segment by the total area of the spectrum, to compensate for the differences in the overall metabolite concentrations within the samples. The resulting data matrices having normalized integral values were exported into Microsoft Office Excel 2007 (Microsoft Corporation, USA). These were further imported to 'The Unscrambler X' Software package (Version 10.0.1, Camo USA, Norway) for multivariate principal component analysis (PCA) and partial least square discriminant analysis (PLS-DA) analysis. PCA was performed on matrices of spectra from CTBL ($n = 72$) and NSCLA ($n = 37$) for comparing their metabolic profiles. In PCA and PLS-DA, a full cross validation using leave-one-out were applied for avoiding the over fitting of the mathematical model. The cross-validation parameter Q^2, indicating the predictability of the model related to its statistical validity, was calculated. An additional cross validation tool, a permutation test, was performed for each model by randomizing the order of Y variables for a specified number of times (Jiang et al. 2013).

After completing the multivariate analysis on the given dataset, about 75 % of the data were randomly selected from Fisher and Yates table (Fisher and Yates 1957) as training set. The training set comprised 81 (CTBL = 54, NSCLA = 27) and the test set comprised 28 (CTBL = 18, NSCLA = 10) NMR spectra out of the total tissue specimens. Another PLS-DA model was generated with the data of the training set. The test set was not included during the construction of the PLS-DA model, but was predicted on the basis of this model. The prediction of the test set for NSCLA or CTBL classes was then compared with their corresponding histopathology reports obtained from the same tissue specimens after HR-MAS NMR analysis.

To validate the process of prediction of any sample, a Receiver Operator Characteristic curve analysis was accomplished on the PLS-DA Factor 1 using SPSS (SPSS Inc., Version 20) software. The ROC curve analysis is considered to be a statistically valid method to evaluate the performance of biomarkers (Søreide 2009; Zweig and Campbell 1993).

3 Results

3.1 Metabolic profile of lymph node tissues

HR-MAS NMR spectra obtained from 109 tissue specimens of patients (109) with enlarged lymph nodes were recorded. Characterization of these metabolites was carried out on the basis of chemical shift, coupling constant and splitting pattern of metabolites as reported in literature (Sitter et al. 2006; Martinez-Granados et al. 2011; Bharti et al. 2013), by comparison with standard NMR spectra of metabolites reported in the biological magnetic resonance bank (BMRB, www.bmrb.wisc.edu), Human Metabolome Data Base (HMDB, www.hmdb.ca) (Markley et al. 2007; Wishart et al. 2009) and earlier published reports on CPMG spectra of tissue metabolites (Schenetti et al. 2006; Griffin and Shockcor 2004).

NMR spectra allowed identification and assignments of 40 endogenous metabolites (Supplementary Table S2). A representative class of CPMG ^{1}H NMR-spectra obtained from CTBL and NSCLA tissue specimens along with their corresponding histopathology of the same specimen is shown in Fig. 1. The histopathology of CTBL samples showed well-formed granuloma composed of central caseation, Langhans giant cells, epithelioid cells and peripheral cuffing of lymphocytes (Asano 2012), while the non-specific ones showed irregularly shaped lymphoid tissues.

3.2 PCA of CTBL and NSCLA NMR spectra

The 3D scatter score plot of PCA showed group separation between CTBL and NSCLA cases (Fig. 2a) thus demonstrating significant metabolic variation among the two groups. A three dimensional scatter plot of the principal components explained 79 % of the variance with the first two explaining 73 % of the total variance. As seen in PC-1 loading plot, the negative loadings of TAG at 1.23 ppm mainly accompanied by mono unsaturated fatty acids (MUFA) (5.4 ppm), PUFA (5.4 ppm) and Tau (3.25, 3.41 ppm) signals positively correlated with CTBL cases and the remaining positive loadings, alanine (Ala), phosphocholine (PCho), glucose (Glc) and lactate (Lac), were associated with NSCLA. The low field signals were found to be insignificant in the loading plot. However, PC-2 loading plot demonstrated positive correlation with

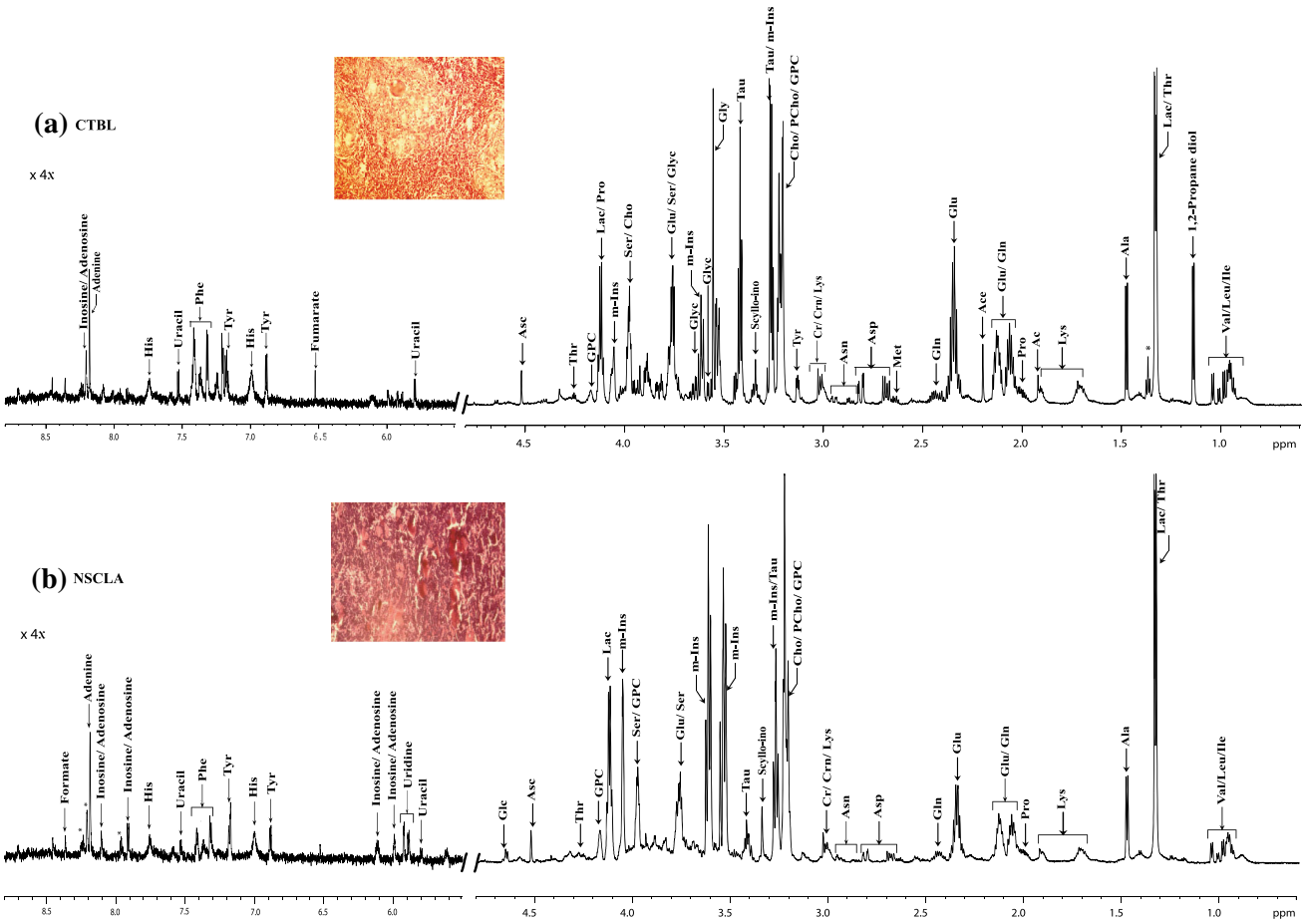

Fig. 1 A typical 800 MHz ^{1}H HR-MAS NMR spectrum of lymph node tissue specimens recorded using CPMG pulse sequence showing assignments of metabolites in **a** 8.80–5.50 and 4.80–0.60 ppm of CTBL; **b** 8.80–5.50 and 4.80–0.60 ppm of NSCLA along with their corresponding histopathological examination images

saturated TAG, PCho, m-Ins, Lac and Glc in NSCLA cases. The remaining negative loadings correlated with CTBL tissue specimens, thus indicating presence of high concentrations of BCAA, Ala, lysine (Lys), Cho, Tau, glycine (Gly) and tyrosine (Tyr). The detailed examination of PC-1 and PC-2 loadings of Fig. 2 showed that the cluster separation is mainly due to PUFA associated with TAG signals (fatty acid; FA); terminal methyl, (–CH_3, 0.90 ppm), saturated methylene (–$(CH_2)_n$, 1.30 ppm), mono-allylic methylene (–CH_2–CH=CH–, 2.05 ppm), di-allylic methylene (–CH=CH–CH_2–CH=CH–, 2.78 ppm), allyl (–CH=CH–, 5.4 ppm), BCAA (0.95–1.05 ppm), Lys (1.72, 1.90, ppm), 1,2-propane diol (1.12 ppm), acetone (Ace) (2.23 ppm), acetate (Ac) (1.92 ppm), ascorbate (Asc) (4.55 ppm), asparagine (Asp) (2.69, 2.82, ppm) His (7.13, 7.98 ppm), Cho, PCho, glycerophosphocholine (GPC) (3.20–3.24 ppm), m-Ins (3.28, 3.54, 3.62, 4.06 ppm), Lac (1.33, 4.12 ppm), Ala (1.48 ppm), creatine/creatinine (Cr/Crn) (3.03 ppm), serine (Ser) (3.85, 3.97 ppm), Gly (3.56 ppm), glycerol (Glyc) (3.56, 3.65, 3.78 ppm), glutamate (Glu) (4.65 ppm).

The PCA of the training set comprising 81 patients were found to be more or less similar to that of the first one. The 3D scatter plot and loading plots of PCA of the training set is shown in Supplementary figure S1 along with its PC1 and PC2 loadings.

3.3 PLS-DA analysis of CTBL and NSCLA cases

PLS-DA facilitated better characterization of the metabolites, distinguishing tubercular and non-tubercular groups from each other. The leave-one-out cross validated 3D score plot showed statistically significant differences between the samples of the two groups (Fig. 3). The PLS-DA model comprising all the tissue specimens was also similar to that of the training set, and both provided 100 % sensitivity and 94.12 % specificity. The R^2 and Q^2 values for both the models were also very close to 1 (0.95, 0.92 and 0.93, 0.88 respectively). The robustness of the PLS-DA model was further grounded by the prediction of the test set with >98 % of accuracy (Fig. 4).

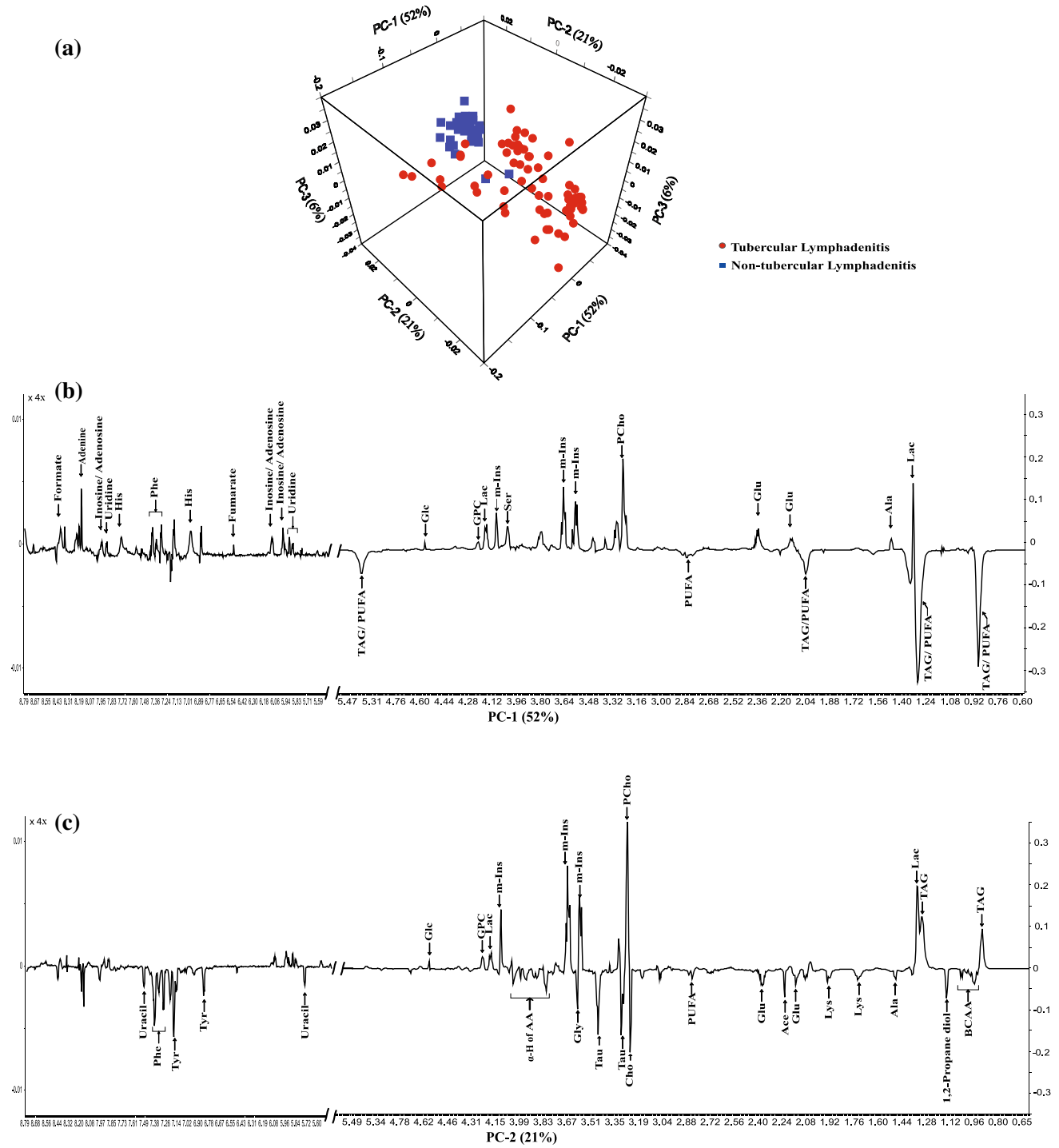

Fig. 2 **a** Three dimensional scattered PCA score plot **b** PC-1 loading **c** PC-2 loading plots of typical ^{1}H HR-MAS NMR spectra of lymph node tissues showing difference in the metabolic profile of non-specific cervical lymphadenitis and cervical tubercular lymphadenitis

3.4 ROC curve analysis

The prediction accuracy of the model was again validated with the area under the curve (AUC) value obtained from the ROC analysis. The value of AUC was found to be identical (0.962) for the total tissue specimens ($n = 109$) (Fig. 5) and the training set ($n = 81$) (Supplementary figure S4) for predicted Y values of PLS-DA model. The ROC calculates the sensitivity and specificity (1-specificity actually) for each cut-off value assuming values that are

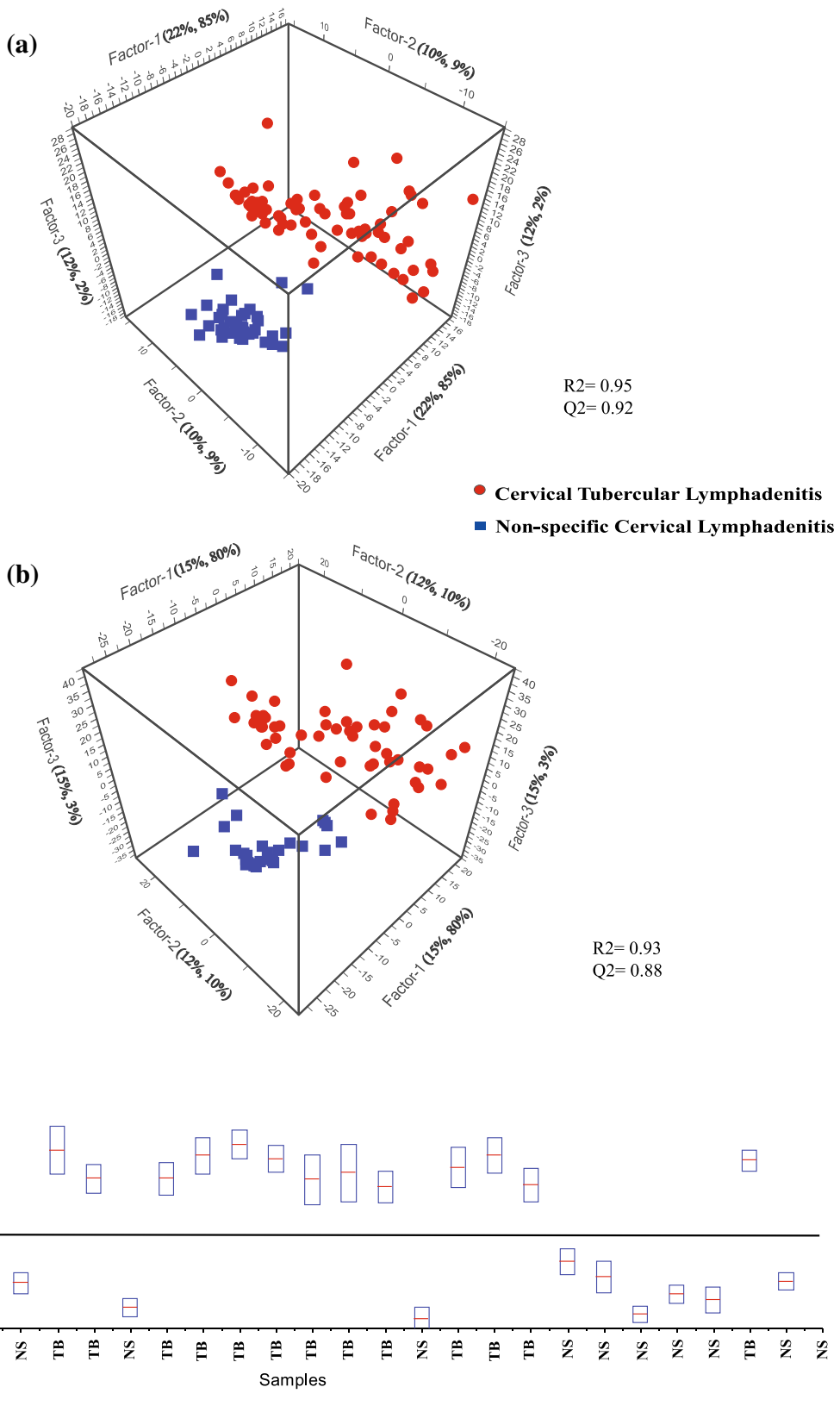

Fig. 3 Comparison of **a** the total ($n = 109$) and **b** the training set ($n = 81$) of 3D-PLS-DA validated score plots showing R^2 and Q^2 values

Fig. 4 Prediction of unknown lymph node tissues (test set, $n = 28$) using PLS model which was prepared using training data set ($n = 81$) samples. The predictions are made on the basis of a priori cut-off value of 0.5 for class membership, using y-predicted box-plot [class 0 for non-specific lymphadenitis (NS) and class 1 for cervical tubercular lymphadenitis (TB)]. The predicted mean values along with standard deviation are depicted

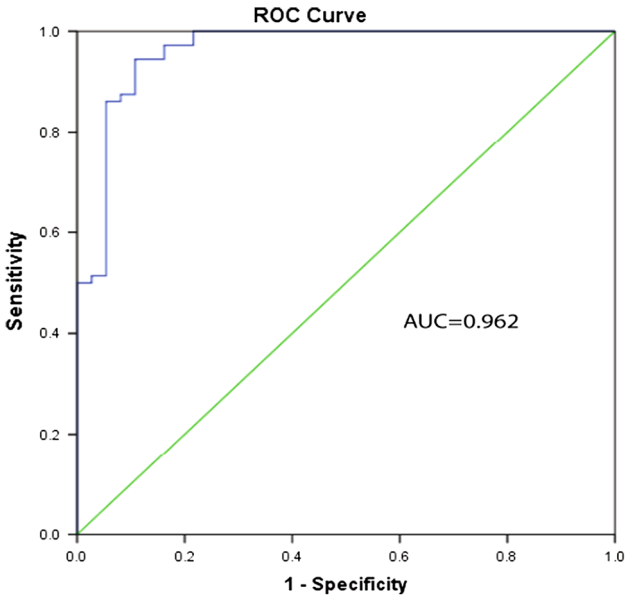

Fig. 5 The ROC curve generated from predicted *Y* values of PLS-DA along with AUC value

equal or above the threshold as positive and those below as negative (Xia et al. 2013). The given ROC curve analysis was found to be near accurate in its sensitivity and specificity.

4 Discussion

The detailed multivariate analysis suggested that majority of the samples in the metabolic profile of CTBL tissues showed the presence of lipids with unsaturated fatty acids (MUFA and PUFA). A comparison of the ^{1}H NMR spectra with pre-saturation of the water resonance using NOESY pulse sequence with CPMG spectra (Supplementary figure S2) indicate that free unsaturated fatty acids are present in abundance in CTBL tissues. The presence of cytoplasmic fatty acids with increased levels of PUFA can be correlated with the earlier studies of lipid metabolism in tumors during cell apoptosis, and necrosis in experimental rat model gliomas which also showed a threefold increase in PUFA levels during the disease (Williams et al. 1998; Hakumaki et al. 1998; Mountford and Wright 1988; Griffin et al. 2003; Griffin and Shockcor 2004). The presence of PUFA seems to be a contribution from host cell metabolites which are released as a result of lipolysis in response to Mtb infection and not by the pathogen. This observation supports the recent findings carried out by earlier workers (Somashekar et al. 2011, 2012) during the progression of Mtb infection in the lungs of a guinea model. They described that possibly an increased level of tumor necrosis factor-α (TNF-α), or presence of Mtb derived phospholipases is responsible for lipolysis during infection. During lipolysis, a remodeling of phospholipids takes place which is induced by the phospholipase enzyme (Vogel 1951). The action of this enzyme yields hydrolysed products like GPC, PCho, Cho and Glyc, which are all distinctively seen in the metabolic profile of lymph node tissues (Figs. 1, 2 and Supplementary figure S5). Although the phospholipase enzymes (viz. phospholipase A and phospholipase C) have been reported to be host derived in tubercular infection (Goldman 1963), yet the possibility of involvement of Mtb derived lipolytic enzymes cannot be ignored. The free fatty acids that are released as a result of lipolysis may act as a source of energy for the pathogen through β-oxidation cycle and glyoxylate shunt (Somashekar et al. 2011). The metabolomic approach in this study was further utilized to study the changes in some low molecular weight metabolites that may be responsible for inducing apoptosis in the CTBL infected tissue specimens. These were Tau, m-Ins and choline containing compounds. Tau, is an indicator of cell apoptosis and is also been suggested as a biomarker of apoptosis in glial tumors (Opstad et al. 2009). It has a dual function of osmoregulation and volume regulation in tissues (Sitter et al. 2010; Srivastava et al. 2011; Wang et al. 2010). It has also been implicated in the mechanism of cell shrinkage during apoptosis in several cell types (Lang et al. 2000; Morán et al. 2000; Friis et al. 2005). Apoptosis produces lipid bodies that show PUFA peaks in the spectra. On the other hand, m-Ins which is mostly found at high levels in brain cells, also acts as an osmolyte, responsible for osmoregulation and volume regulation in the body. In earlier studies, m-Ins had been proved to be essential for the survival and growth of cultured human cells (normal or malignant), where the growth completely ceased in m-Ins deficient media, resulting in cell injury and eventually leading to cell death (Eagle et al. 1957), therefore it has been implicated for cell growth (Ross 1991). We can thus imply that Tau and m-Ins when present at their threshold concentrations were responsible for osmoregulation and volume regulation. But during the course of infection, increase in the concentration of Tau with simultaneous decrease in m-Ins levels (which is quite evident from the PC loadings) induces cell apoptosis in the infected tissues, eventually leading to cell death and necrosis. These in turn result in the accumulation of lipids that remain even after cell death, (Griffin et al. 2003) which further reinstates the presence of mobile fatty acids/lipids in CTBL cases. Moreover, the increase in the levels of Cho can be considered as a signature for lipolysis. Generally, during lipolysis PCho and GPC levels also increase along with Cho (Podo 1999) but, on the contrary, in the present study Cho was found elevated, while PCho and GPC were down regulated in CTBL cases. The reason remains uncertain but this may be due to alteration in the metabolic processes during Mtb infection.

The other low molecular weight metabolites that were present in TBL samples were masked by the presence of lipids and could not be seen in PC-1 loadings. However, PC-2 loadings despite of less explained variance (21 %) clearly displayed the presence of small metabolites in CTBL cases. Although lipid signals are also seen in case of NSCLA tissues, but they were mostly saturated lipids in the PC-2 loading plot. The negative loadings correlating with CTBL could act as useful markers in identifying the disease. These are BCAA, Ala, Ace, Lys, Glu, Gly, Tyr and 1, 2-propane diol and were found be to be elevated. The increased levels of BCAA, Ala and Gly along with Glu and Asp indicates the involvement of glycolysis and protein degradation (Yang et al. 2007) because of chronic granulomatous inflammation. The presence of 1,2-propanediol can be the result of altered glycerol metabolism (Michal 1998). The relative concentration of Lac and Glc was found to be more in NSCLA, as evident in the PC-1 and PC-2 loadings. This finding may be an indication of hypoxia i.e. anaerobic glycolysis (Via et al. 2008) which is predominant in NSCLA cases.

The presence of additional resonances in the aromatic region (7.0–7.5 ppm) in only 35 tissue specimens of CTBL cases could not be ascertained. A representative stack plot of twenty spectra demonstrating the presence of additional resonances in the aromatic region is shown in Supplementary figure S3. The possibility of the presence of discrete form of phenolic glycolipids (PGL), an integral membrane structure component of Mtb cannot be ruled out (Subramanian et al. 2008). The possible presence of PGL needs to be ascertained because this may provide a correlation with duration and/or the intensity of the Mtb infection.

The results of multivariate statistical analyses provide a lead in the identification of CTBL samples non-invasively. The score plot and loading plots in PCA, as discussed above, clearly differentiate between the metabolic profile of the two mentioned classes, and PLS-DA allowed a precise prediction of the dataset. The value for R^2 for the PLS-DA model, as shown in Fig. 3, was found to be very close to 1 ($\sim$0.95), which indicates that the present model is quite robust with least overfitting and having a Q^2 of 92 % predictive ability. The R^2 value for the training set was $\sim$0.93 with $Q^2 \sim 0.88$. In order to reinstate the robustness and the predictive ability of the PLS-DA model, the test set was predicted for classification. The prediction table in Fig. 4 clearly segregates the CTBL samples from those of NSCLA, and all the samples were found to be predicted correctly when compared with their corresponding histopathological results. Thus the PLS-DA model generated in the present study had correctly classified and predicted the samples for CTBL ($n = 72$) and NSCLA ($n = 37$) with >98 % of correct classification and $\sim$100 % predictive accuracy. Further, to probe the discriminating ability of PLS-DA model, ROC curve showed AUC value of 0.962, which further validated the discrimination of CTBL class from NSCLA cases.

5 Conclusion

HR-MAS NMR spectroscopy is good option for evaluating the metabolic profile of tubercular lymph node tissues and their differential diagnosis. We believe that HR-MAS NMR spectroscopy may be used as an efficient and alternative diagnostic method for initiating anti-tubercular treatment in patients suffering from cervical TB lymphadenitis. However, a large sample size is required which is mandatory for such an endeavor for categorizing the extent of associated pathology in Mtb infected cervical lymph nodes. The above mentioned biomarkers, mainly Tau, m-Ins and choline containing compounds, may further be explored using in vivo single-voxel MR spectroscopy non-invasively for differentiating cervical TB.

Acknowledgments The contribution of the Department of Surgery and Department of Pathology, King George's Medical University, Lucknow for the present study is gratefully acknowledged. Dr. Suruchi Singh and Ms. Shatakshi Srivastava gratefully acknowledge CSIR for providing the fellowship.

References

Ahuja, A. T., Ying, M., & Wang, K. T. (2008). Ultrasound of malignant lymph nodes. *Cancer Imaging, 8*(1), 18–58.

Asano, S. (2012). Granulomatous Lymphadenitis. *Journal of Clinical and Experimental Hematopathology, 52*(1), 1–16.

Attie, J. N., Setzin, M., & Klein, L. (1993). Thyroid carcinoma presenting as an enlarged cervical lymph node. *American Journal of Surgery, 166*(4), 428–430.

Beckonert, O., Coen, M., Keun, H. C., Wang, Y., Ebbels, T. M., Holmes, E., et al. (2010). High-resolution magic-angle spinning NMR spectroscopy for metabolic profiling of intact tissues. *Nature Protocols, 5*(6), 1019–1032.

Bharti, S. K., Behari, A., Kapoor, V. K., Kumari, N., Krishnani, N., & Roy, R. (2013). Magic angle spinning NMR spectroscopic metabolic profiling of gall bladder tissues for differentiating malignant from benign disease. *Metabolomics, 9*, 101–118.

Cheng, L. L., Chang, I. W., Louis, D. N., & Gonzalez, R. G. (1998). Correlation of high-resolution magic angle spinning proton magnetic resonance spectroscopy with histopathology of intact human brain tumor specimens. *Cancer Research, 58*(9), 1825–1832.

Choi, J. S., Baek, H.-M., Kim, S., Kim, M. J., Youk, J. H., Moon, H. J., et al. (2012). HR-MAS MR spectroscopy of breast cancer tissue obtained with core needle biopsy: Correlation with prognostic factors. *PLoS ONE, 7*(12), e51712.

Corbett, E. L., Watt, C. J., Walker, N., Maher, D., Williams, B. G., Raviglione, M. C., et al. (2003). The growing burden of tuberculosis: Global trends and interactions with the HIV epidemic. *Archives of Internal Medicine, 163*(9), 1009–1021.

Davies, M., Arumugam, P. J., Shah, V. I., Watkins, A., Morgan, A. R., Carr, N. D., et al. (2008). The clinical significance of lymph node micrometastasis in stage I and stage II colorectal cancer. *Clinical and Translational Oncology, 10*(3), 175–179.

De Cock, K. M. (2006). HIV infection, tuberculosis and World AIDS Day. *International Journal of Tuberculosis and Lung Disease, 10*, 1305.

Duportet, X., Aggio, R., Carneiro, S., & Villas-Boas, S. (2011). The biological interpretation of metabolomic data can be misled by the extraction method used. *Metabolomics, 8*(3), 410–421.

Eagle, H., Oyama, V. I., Levy, M., & Freeman, A. E. (1957). Myo-inositol as an essential growth factor for normal and malignant human cells in tissue culture. *The Journal of Biological Chemistry, 226*, 191–205.

Eshete, A., Zeyinudin, A., Ali, S., Abera, S., & Mohammed, M. (2011). *M. tuberculosis* in lymph node biopsy Paraffin-embedded sections. *Tuberculosis Research and Treatment, 2011*, 127817.

Fisher, R. A., & Yates, F. (1957). *Statistical tables for biological, agricultural, and medical research* (5th ed.). Edinburgh: Oliver and Boyd.

Friis, M. B., Friborg, C. R., Schneider, L., Nielsen, M. B., Lambert, I. H., Christensen, S. T., et al. (2005). Cell shrinkage as a signal to apoptosis in NIH 3T3 fibroblasts. *The Journal of Physiology, 567*(2), 427–443.

Geldmacher, H., Taube, C., Kroeger, C., Magnussen, H., & Kirsten, D. K. (2002). Assessment of lymph node tuberculosis in Northern Germany: A clinical review. *Chest, 121*(4), 1177–1182.

Giskeødegard, G. F., Grinde, M. T., Sitter, B., Axelson, D. E., Lundgren, S., Fjøsne, H. E., et al. (2010). Multivariate modeling and prediction of breast cancer prognostic factors using MR metabolomics. *Journal of Proteome Research, 9*, 972–979.

Global Tuberculosis control, WHO report 2009 (pp. 76). Geneva.

Goldman, D. S. (1963). Enzyme systems in the Mycobacteria. XV. Initial steps in the metabolism of glucose. *Journal of Bacteriology, 86*(1), 30–37.

Griffin, J. L., Lehtimäki, K. K., Valonen, P. K., Gröhn, O. H. J., Kettunen, M. I., Ylä-Herttuala, S., et al. (2003). Assignment of ^{1}H nuclear magnetic resonance visible polyunsaturated fatty acids in BT4C gliomas undergoing ganciclovir-thymidine kinase gene therapy-induced programmed cell death. *Cancer Research, 63*, 3195–3201.

Griffin, J. L., & Shockcor, J. P. (2004). Metabolic profiles of cancer cells. *Nature Reviews Cancer, 4*(7), 551–561.

Gupta, R. K., Husain, N., Kathuria, M. K., Datta, S., Rathore, R. K., & Husain, M. (2001). Magnetization transfer MR imaging correlation with histopathology in intracranial tuberculomas. *Clinical Radiology, 56*(8), 656–663.

Gupta, R. K., & Roy, R. (1999). MR Imaging and spectroscopy of intracranial tuberculoma. *Current Science, 76*, 783–788.

Hakumaki, J. M., Poptani, H., Puumalainen, A.-M., Loimas, S., Paljärvi, L. A., Ylä-Herttuala, S., et al. (1998). Quantitative ^{1}HNMR diffusion spectroscopy of BT4C rat glioma during thymidine kinase-mediated gene therapy in vivo: Identification of apoptotic response. *Cancer Research, 58*(17), 3791–3799.

Jain, A. (2011). Extra pulmonary tuberculosis: A diagnostic dilemma. *Indian Journal of Clinical Biochemistry, 26*(3), 269–273.

Jiang, C. Y., Yang, K. M., Yang, L., Miao, Z. X., Wang, Y. H., & Zhu, H. B. (2013). A ^{1}H NMR-based metabolomic investigation of time-related metabolic trajectories of the plasma, urine and liver extracts of hyperlipidemic hamsters. *PLOS ONE, 8*(6), 1–20.

Lang, F., Madlung, J., Siemen, D., Ellory, C., Lepple-Wienhues, A., & Gulbins, E. (2000). The involvement of caspases in the CD95(Fas/Apo-1)- but not swelling induced cellular taurine release from Jurkat T-lymphocytes. *Pflugers Archives, 440*(1), 93–99.

Lindberg, R. (1972). Distribution of cervical lymph node metastases from squamous cell carcinoma of the upper respiratory and digestive tracts. *Cancer, 29*(6), 1446–1449.

Markley, J. L., Anderson, M. E., Cui, Q., Eghbalnia, H. R., Lewis, I. A., Hegeman, A. D., et al. (2007). New bioinformatics resources for metabolomics. *Pacific Symposium on Biocomputing, 12*, 157–168.

Martinez-Granados, B., Morales, J. M., Rodrigo, J. M., Del Olmo, J., Serra, M. A., Ferrandez, A., et al. (2011). Metabolic profile of chronic liver disease by NMR spectroscopy of human biopsies. *International Journal of Molecular Medicine, 27*(1), 111–117.

Michal, G. (1998). On representation of metabolic pathways. *Biosystems, 47*, 1–7.

Morán, J., Hernandez-Perch, X., Merchant-Larios, H., & Pasantes-Morales, H. (2000). Release of taurine in apoptotic cerebellar granule neurons in culture. *Pflugers Archives, 439*(3), 271–277.

Mountford, C. E., & Wright, L. C. (1988). Organisation of lipids in the plasma membranes of malignant and stimulated cells: A new model. *Trends in Biochemical Sciences, 13*(5), 172–177.

Opstad, K. S., Bell, B. A., Griffiths, J. R., & Howe, F. A. (2009). Taurine: A potential marker of apoptosis in gliomas. *British Journal of Cancer, 100*(5), 789–794.

Podo, F. (1999). Tumour phospholipid metabolism. *NMR in Biomedicine, 12*, 413–439.

Purohit, M. R., Mustafa, T., Wiker, H. G., Morkve, O., & Sviland, L. (2007). Immunohistochemical diagnosis of abdominal and lymph node tuberculosis by detecting *Mycobacterium tuberculosis* complex specific antigen MPT64. *Diagnostic Pathology, 2*(36), 1–9.

Ross, B. D. (1991). Biochemical considerations in 1H spectroscopy. Glutamate and glutamine; myo-inositol and related metabolites. *NMR in Biomedicine, 4*, 59–63.

Schenetti, L., Mucci, A., Parenti, F., Cagnoli, R., Righi, V., Tosi, M. R., et al. (2006). HR-MAS NMR spectroscopy in the characterization of human tissues: Application to healthy Gastric mucosa. *Concepts in Magnetic Resonance Part A, 28A*(6), 430–443.

Shahzad, A., & Kohler, G. (2009). Tuberculous cervical lymphadenitis in developing countries: A challenging infectious disease. *Vaccine, 27*(42), 5731.

Sitter, B., Bathen, T. F., Singstad, T. E., Fjosne, H. E., Lundgren, S., Halgunset, J., et al. (2010). Quantification of metabolites in breast cancer patients with different clinical prognosis using HR MAS NMR spectroscopy. *NMR in Biomedicine, 23*(4), 424–431.

Sitter, B., Lundgren, S., Bathen, T. F., Halgunset, J., Fjosne, H. E., & Gribbestad, I. S. (2006). Comparison of HR MAS NMR spectroscopic profiles of breast cancer tissue with clinical parameters. *NMR in Biomedicine, 19*(1), 30–40.

Somashekar, B. S., Amin, A. G., Rithner, C. D., Troudt, J., Basaraba, R., Izzo, A., et al. (2011). Metabolic profiling of lung granuloma in *Mycobacterium tuberculosis* infected guinea pigs: Ex vivo ^{1}H magic angle spinning NMR studies. *Journal of Proteome Research, 10*, 4186–4195.

Somashekar, B. S., Amin, A. G., Tripathi, P., MacKinnon, N., Rithner, C. D., Shanley, C. A., et al. (2012). Metabolic signatures in guinea pigs infected with epidemic-associated W-Beijing strains of *Mycobacterium tuberculosis*. *Journal of Proteome Research, 11*, 4873–4884.

Srivastava, S., Roy, R., Gupta, V., Tiwari, A., Srivastava, A. N., & Sonkar, A. A. (2011). Proton HR-MAS NMR spectroscopy of oral squamous cell carcinoma tissues: An ex vivo study to identify malignancy induced metabolic fingerprints. *Metabolomics, 7*(2), 278–288.

Subramanian, A., Gupta, A., Saxena, S., Gupta, A., Kumar, R., Nigam, A., et al. (2005). Proton MR CSF analysis and a new software as predictors for the differentiation of meningitis in children. *NMR in Biomedicine, 18*, 213–225.

Subramanian, A., Joshi, B. S., Roy, A. D., Roy, R., Gupta, V., & Dang, R. S. (2008). NMR spectroscopic identification of cholesterol esters, plasmogen and phenolic glycolipids as fingerprint markers of human intracranial tuberculomas. *NMR in Biomedicine, 21*, 272–288.

Søreide, K. (2009). Receiver-operating characteristic curve analysis in diagnostic, prognostic and predictive biomarker research. *Journal of Clinical Pathology, 62*, 1–5.

Thangappah, R. B. P., Paramasivan, C. N., & Narayanan, S. (2011). Evaluating PCR, culture and histopathology in the diagnosis of female genital tuberculosis. *Indian Journal of Medical Research, 134*(1), 40–46.

Uphoff, C. C., & Drexler, H. G. (2011). Detecting mycoplasma contamination in cell cultures by polymerase chain reaction. *Methods in Molecular Biology, 731*, 93–103.

Via, L. E., Lin, P. L., Ray, S. M., Carrillo, J., Allen, S. S., Eum, S. Y., et al. (2008). 3rd Tuberculous granulomas are hypoxic in guinea pigs, rabbits, and nonhuman primates. *Infection and Immunity, 76*(6), 2333–2340.

Vogel, F. S. (1951). A lipolytic enzyme in reactive histocytes of Guinea pigs with experimental encephalomyelitis. *The Journal of Experimental Medicine, 93*(4), 305–312.

Wang, H., Tso, V. K., Slupsky, C. M., & Fedorak, R. N. (2010). Metabolomics and detection of colorectal cancer in humans: A systematic review. *Future Oncology, 6*(9), 1395–1406.

Williams, S. N. O., Antony, M. L., & Brindle, K. M. (1998). Induction of apoptosis in two mammalian cell lines results in increased levels of fructose-1,6-phosphate and CDP-choline as determined by ^{31}P MRS. *Magnetic Resonance in Medicine, 40*(3), 411–420.

Wishart, D. S., Knox, C., Guo, A. C., Eisner, R., Young, N., Gautam, B., et al. (2009). HMDB: A knowlegde base for the human metabolome. *Nucleic Acids Research, 37*(Database issue), D603–D610.

Wong, E. B., Cohen, K. A., & Bishai, W. R. (2013). Rising to the challenge: New therapies for tuberculosis. *Trends in Microbiology, 21*(9), 493–501.

World Health Organization. Global tuberculosis control 2010. (pp. 5–7). Geneva.

Wright, C. A., Van der Burg, M., Geiger, D., Noordzij, J. G., Burgess, S. M., & Marais, B. J. (2008). Diagnosing mycobacterial lymphadenitis in children using fine needle aspiration biopsy: Cytomorphology, ZN staining and autofluorescence-making more of less. *Diagnostic Cytopathology, 36*(4), 245–251.

Xia, J., Broadhurst, D. I., Wilson, M., & Wishart, D. S. (2013). Translational biomarker discovery in clinical metabolomics: An introductory tutorial. *Metabolomics, 9*(2), 280–299.

Yang, Y., Li, C., Nie, X., Feng, X., Chen, W., Yue, Y., et al. (2007). Metabonomic studies of human hepatocellular carcinoma using high-resolution magic-angle spinning 1H NMR spectroscopy in conjunction with multivariate data analysis. *Journal of Proteome Research, 6*(7), 2605–2614.

Zhang, M., Li, M., Xu, G.-P., & Liu, H.-J. (2011). Neoplasm-like abdominal nonhematogenous disseminated tuberculous lymphadenopathy: CT evaluation of 12 cases and literature review. *World Journal of Gastroenterology, 17*(35), 4038–4043.

Zweig, M. H., & Campbell, G. (1993). Receiver-operating characteristic (ROC) plots: A fundamental evaluation tool in clinical medicine. *Clinical Chemistry, 39*(4), 561–577.